UDC 539.4

Accelerated Life Test and FEM Simulation-Based Fatigue Analysis of an Aluminum Alloy Push Rod

L. Xu[a,1] and G. Z. Dai[b]

[a] School of Material Science and Engineering, Xihua University, Chengdu, China

[b] School of Material Science and Engineering, Southwest Jiaotong University, Chengdu, China

[1] flyagainstwater@163.com

The accelerated life test based on the spectrum of fatigue loads was used both in numerical simulation and bench tests of the push rod. The symmetrical cycling of the push rod was presented as the positive pulsating load spectrum corresponding to the stress spectrum of the critical node in the finite element model. As FEM analysis demonstrates, the fatigue crack initiation would occur at the edge of the first-position pin hole with maximum stress and minimum fatigue life. Bench test results show that the fatigue crack initiation and fatigue life of the push rod are in good agreement with FEM data.

Keywords: high-strength aluminum alloy, push rod, accelerated life test, fatigue life, finite element analysis.

Introduction. Train's traction structural parts subjected to the variable loading may tend to fatigue failure during the high-speed operation. The fatigue failure prevents the components from functioning properly, and causes the critical problems in vehicle safety [1, 2]. Therefore, in order to secure the trains components against fatigue failures, durability test of the components has been performed in the vehicle industries [3]. At present, analysis of fatigue and durability are used to the most components which is the basic guarantee of the vehicle secure operation. The fatigue analysis is usually carried out by theoretical calculation and bench tests [4, 5].

Push rod in the bogie system transmits tractive force between axle box and frame of bogie which is shown in Fig. 1. In order to evaluate the fatigue life of the push rod assembly in the bogie and saving testing time, the accelerated fatigue analysis of the push rod was performed by the finite-element method (FEM) analysis and high-cycle fatigue test of the Al–Zn–Mg–Cu alloy. Predicted accelerated fatigue life of the push rod was compared with the bench test determined damage fatigue life to verify the validity of the FEM results.
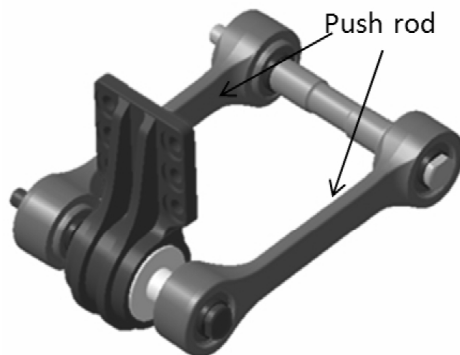

Fig. 1. Push rod assembly in bogie system of CRH5.

1. **Material**. The push rod was made from Al–6.2Zn–2.2Mg–1.6Cu alloy. According to the material micrograph depicted in Fig. 2, a typical microstructure of this aluminum alloy contains elongated band-like grains aligned in the rod length direction. To research the mechanical properties of the alloy, cylindrical specimens with a diameter of 8 mm were taken from the push rod. Material testing machine with 200 kN capability was employed for the static tensile test. Mechanical properties of the alloy are shown in Table 1.

T a b l e 1
Mechanical Properties of Al–6.2Zn–2.2Mg–1.6Cu Alloy

Elastic modulus E, GPa	71
Poisson's ratio υ	0.33
Yield strength σ_s, MPa	460
Tensile strength σ_b, MPa	570
Elongation ψ, %	9.7

High-frequency fatigue testing machine was employed for the axial loading fatigue test. The fatigue life of the aluminum alloy can be described by the Basquin equation as follows:

$$\lg \sigma_{-1} = 3.27 - 0.12 \lg N_f, \tag{1}$$

where σ_{-1} is fatigue stress limit and N_f is fatigue life.
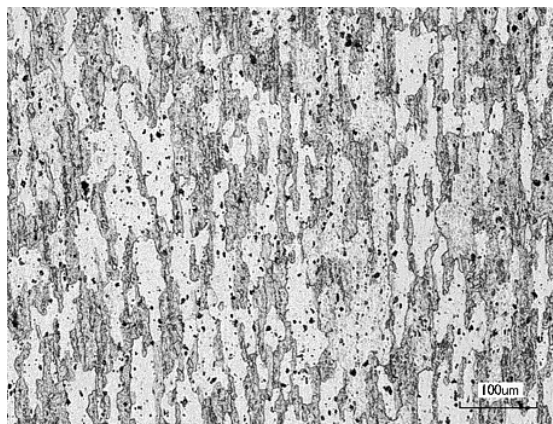

Fig. 2. Metallographic microstructure of Al–Zn–Mg–Cu alloy.

2. **Numerical Analysis**. Fatigue life of each structure depends on the fatigue strength of material and the operating loads of the components. Fatigue cracking originates in the weakest region with the maximum stress amplitude. Therefore, in order to analyze the fatigue cracking behavior and predict the fatigue life of a component, stress analysis at the critical region is necessary.

As the first step in the numerical fatigue analysis, a finite-element model of the push rod assembly was created in ANSYS® v12.0 commercial FEM analysis software as shown in Fig. 3. Solid185 hexahedral elements are used for building the push rod meshed model.

2.1. *Stress analysis under Various Tensile and Compressive Loads*. The equivalent stress (assessed via the von Mises strength criterion) in the push rod generated by the tensile load of 27.2 kN, which is fourfold of the normal service load, is shown in Fig. 4a.
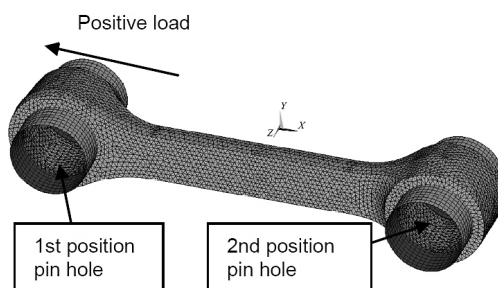
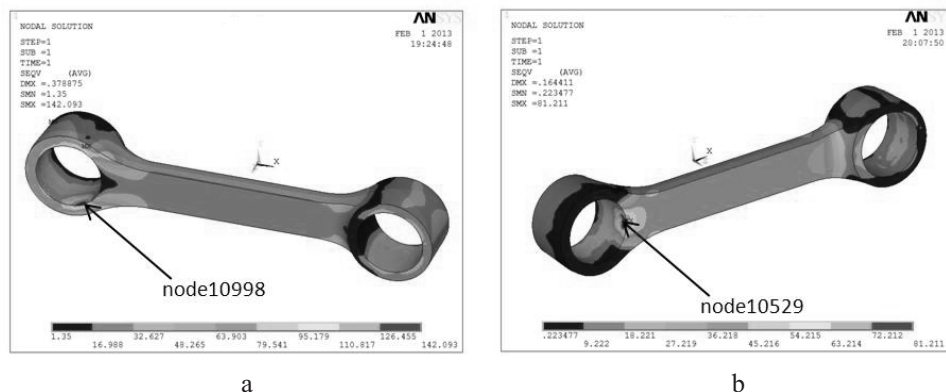Fig. 3. FEM model of the push rod.

a

b

Fig. 4. The equivalent (von Mises) stress distribution of a push rod under the tensile (a) and compressive (b) load of 27.2 kN.

The stress distribution of the both pin holes is different due to the asymmetric structure. Two inner wall areas of the first location pin hole marked in red in Fig. 4a exhibit a similar maximum level of equivalent stress of about 142 MPa, while the maximum principal stress is 149 MPa.

The equivalent stress in the push rod due to a compressive load of 27.2 kN is shown in Fig. 4b. Inner wall areas of the first location pin hole (which is marked in red) are subjected to the equivalent stress of about 77.3 MPa, while the maximum principal stress is 6.5 MPa.

The stressed state and stress amplitude are essential to choose the fatigue failure criterion. Table 2 shows that the intermediate and the minimum principal stress of node 10998 is close to zero, while the maximum principal stress is close to the equivalent stress. Hence, node 10998 can be considered to be subjected to uniaxial tensile stress of about 147.8 MPa. The stress in node 10998 is close to zero under the compressive load of 27.2 kN. Thus, the compressive load does not contribute to the fatigue of this node 10998, and the fatigue analysis can be based on the maximum principal stress criterion.

T a b l e 2

The Stresses (MPa) of the Node 10998 at the Tensile Load of 27.2 kN

Load type	σ_{eq}	σ_1	σ_2	σ_3	σ_x
Tensile	142.9	147.8	8.2	3.4	127.8
Compressive	0.5	0.1	-0.1	-0.5	-0.4

The Stresses (MPa) of the Node 10529 at the Compressive Load of 27.2 kN

Load type	σ_{eq}	σ_1	σ_2	σ_3	σ_y
Tensile	22.0	-2.8	-4.4	-25.8	-24.6
Compressive	77.3	6.5	-19.9	-80.6	6.0

Table 3 shows that node 10529 is in the triaxial compressive stressed state under the tensile loading of 27.2 kN. But since both the maximum and intermediate principal stresses approach zero, the stress in node 10529 can be reduced to uniaxial compressive stress of about 24.6 MPa, while this node experiences a biaxial compressive stress under the compressive load of 27.2 kN.

Connelly and Davis [6] introduced the triaxiality factor (TF) to determine the stressed state:

$$TF = \frac{I_1}{\sigma_{eq}}, \qquad (2)$$

where I_1 represents the first stress invariant.

In node 10998 under the tensile load of 27.2 kN, $TF = 1.1$. Since it approximately equals to unity, the uniaxial tensile stress criterion can be used for this node. Comparing the stress amplitude of the maximum stresses in nodes 10998 and 10529, in the case where the push rod is subjected to cyclic symmetric tension-compression (i.e., with stress ratio $R = -1$), node 10998 endures the critical fatigue stress cyclic load. Then, the fatigue analysis of the push rod can be reduced to the loading scheme shown in Fig. 5, which implies that node 10998 endures the uniaxial tensile stress with the most critical fatigue stress spectrum.
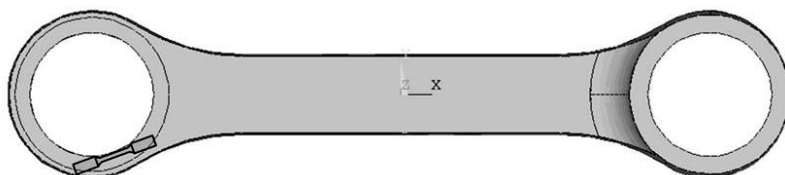

Fig. 5. The critical node 10998 subjected to uniaxial fatigue under a symmetrical cyclic load.

2.2. ***ALT Fatigue Testing Spectrum***. Accelerated life test (ALT) of products and materials is used to get information quickly on their life distributions [7]. Such testing involves subjecting the test units to conditions that are more severe than normal ones and yields shorter fatigue lives than those under regular conditions. The data obtained at more severe or accelerated conditions are extrapolated by means of an appropriate model to obtain an estimate of the life distribution under the normal conditions. ALT provides savings in time and cost, as compared to testing under the normal conditions. This paper presents ALT of the push rod, which is used to identify the product weak parts and predict its fatigue life.

Firstly, it is necessary to study the failure mechanism of the push rod via ALT fatigue testing loading. The stress of the characteristic nodes 10998 and 10592 changes with a series of lo as shown in Fig. 6. The stresses in the characteristic nodes are related to loads by a linear relationship. The stress state of the two nodes remains unchanged with the load variation. Figure 6a shows that the equivalent stress is primarily constituted by the maximum principal stress, which direction nearly coincides with the x axis. Figure 6b
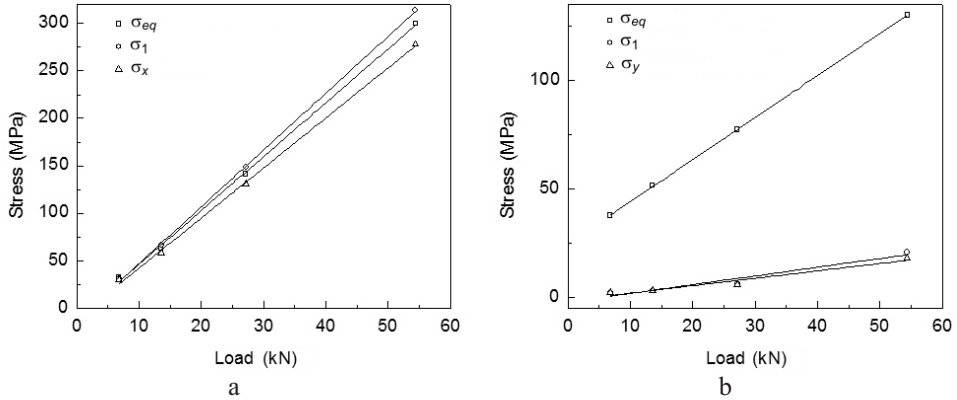
Fig. 6. Stress variation for loads ranging from 6.8 to 54.4 kN in nodes 10998 (a) and 10529 (b).

shows that the maximum principal stress approaches zero, so that the equivalent stress is mainly constituted by the compressive stress. Above all, the fatigue failure mechanism of the push rod would not change with the load variation from 27.2 to 54.4 kN.

Secondly, it is necessary to simplify the loading spectrum of the bench test, in order to improve the prediction efficiency. The symmetric sine load spectrum of the rod is shown in Fig. 7a. The corresponding stress spectrum of node 10998 is the pulsating stress spectrum, while the push rod is under the symmetric sine load spectrum depicted in Fig. 7b. The fatigue spectrum of 10998 node in Fig. 7b is equal to that in Fig. 7d, so the load spectrum of the push rod can be reduced to that in Fig. 7c. Above all, the critical maximum principal stress amplitude of the rod is at node 10998. To save the fatigue bench test time, the fatigue load spectrum could be set as a pulsing tensile load, as is shown in Fig. 7c.
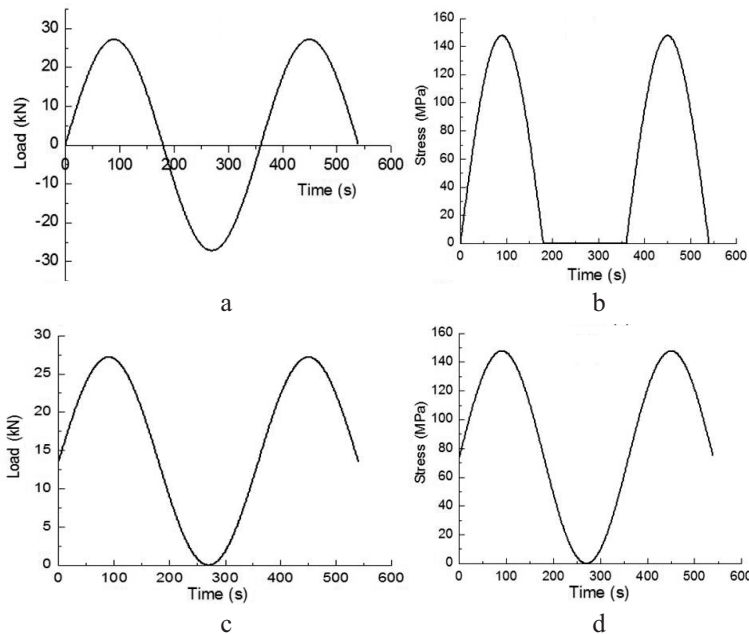

Fig. 7. Load spectrum of the rod and stress spectrum of node 10998: (a) symmetric sine load spectrum of the rod at 27.2 kN; (b) stress spectrum of node 10998 under symmetric sine load spectrum of the rod at 27.2 kN; (c) pulsating sine load spectrum of the rod at 27.2 kN; (d) stress spectrum of node 10998 under pulsating sine load spectrum of the rod at 27.2 kN.

2.3. ***FEM Fatigue Analysis Results***. Fatigue analysis was carried out by the FEM. The surface and scale factor were set at 1.5, according to the surface processing state. Figure 8 shows that the crack initiation may occur in the critical zone at the inner wall of the first pin hole surface. For the maximum stress and minimum fatigue life in Figs. 4 and 8, the crack propagation begins at this area according to the FEM analysis. The respective fatigue life is assessed as $3 \cdot 10^5$ cycles under a pulsing tensile load of 52 kN.
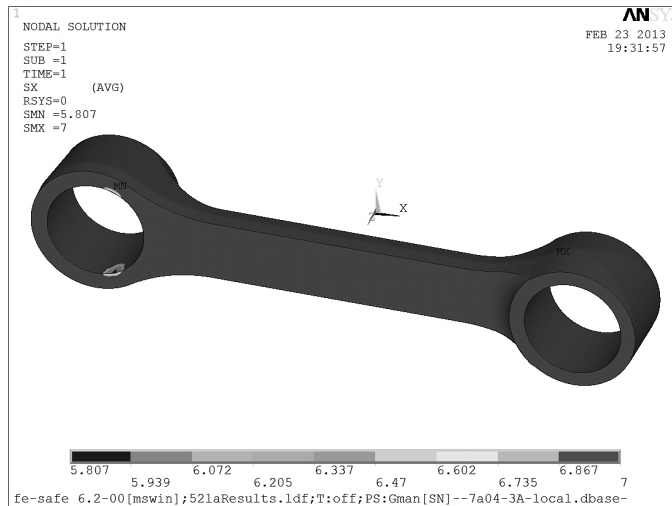

Fig. 8. Calculated stresses in the rod under a pulsing tensile load of 52 kN.

3. **Bench Fatigue Test and Failure Analysis**. The load capacity and fatigue behavior of the push rod under dynamic loads are determined by the tractive force fatigue tests shown in Fig. 9. In these tests, the push rod and pin joint assembly are positioned on a vertical actuator. The pulsating sine spectrum load of 10 Hz is applied to the first position pin along the axial direction of the actuator.
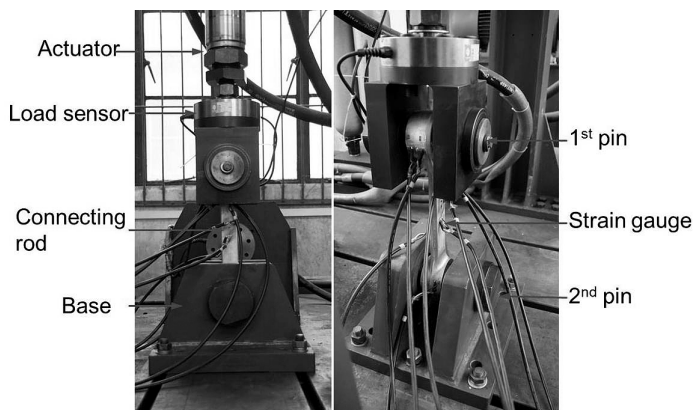

Fig. 9. Electrohydraulic servo used for bench test.

In order to verify the static FEM simulation results, local stresses were measured by the strain gauge testing method, as shown in Fig. 10. The data summarized in Table 4 strongly indicate that the FEM calculated results are in good agreement with strain gauge testing results with a tensile load of 52 kN. By carrying out the fatigue bench tests with the

T a b l e 4

Local Stresses (MPa) in the Rod under a Tensile Load of 52 kN

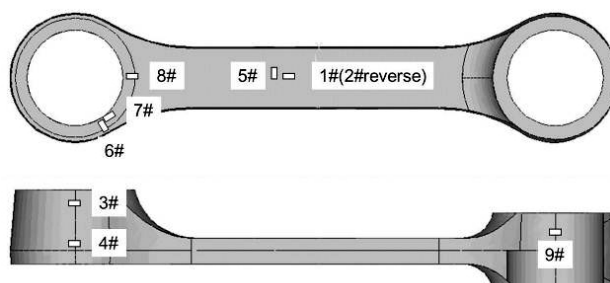| Location	1	2	3	4	6	7	8
Experimental	52.6	110	−23.1	35.2	−64.6	109	0.71
FEM	56.1	99.6	−14.2	64.3	−11.5	135	−0.52

Fig. 10. Sensors' locations on the push rod.

pulsating load of 26 kN, the load life curve of the push rod was determined and used for assessing the experimental fatigue life.

Figure 11 indicates that a fatigue crack was initiated at the inner pinhole edge of the push rod, and propagated through the cross-sectional area of the first position pinhole. The ductile mode of fracture in the final fracture zone can be readily observed in Fig. 12.
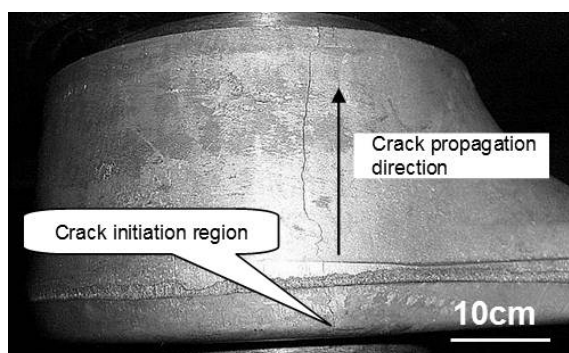

Fig. 11. Fracture appearance of the rod with the load of 52 kN.

The micrograph zone located within the white box in Fig. 12 is enlarged in Fig. 13, to confirm the fatigue crack propagating path. Thus, Fig. 13 shows the crack propagation zone, with the fatigue propagation characteristics represented by fatigue striations of a micron scale. When tensile forces are repeatedly applied to the structure parts, the crack jumps at a small distance to form the advance striation. With striations perpendicular to the fatigue crack propagation direction, the fatigue crack direction is shown as a white arrow. Therefore, the fatigue crack initiated at the inner wall of the pin hole and propagated along the radial or axial direction, finally resulting in the fracture failure at the pinhole wall.

Figure 14 shows that predicted fatigue life of the push rod by FEM agreed fairly well with the experimental life within three times.

Comparing the fatigue life results for the first- and second-location pinholes, that the latter is more than one hundred times longer than that of the former. In order to increase the
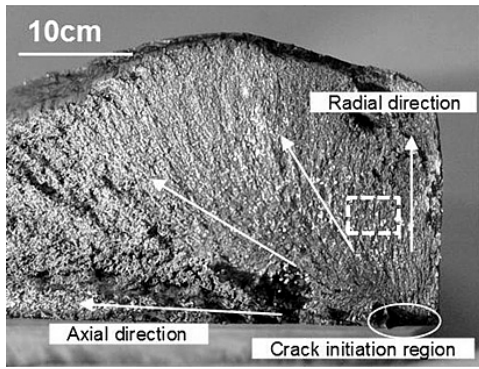
Fig. 12   Fig. 13

Fig. 12. Fracture macrograph of the rod.
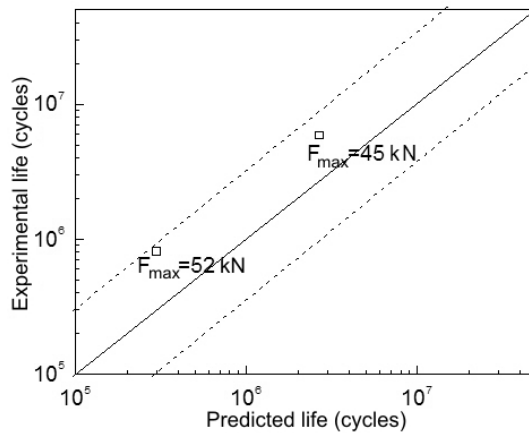Fig. 13. LSCM micrograph showing the crack propagation.

Fig. 14. FEM-calculated life vs. test fatigue life.

fatigue life of the push rod, it is necessary to reduce the stress concentration in the critical zones.

Conclusions. Fatigue analysis of the push rod was carried out using a comprehensive combination of the Al–Zn–Mg–Cu alloy characterization, FEM simulation, bench test, and ALT fatigue life evaluation. It was concluded that:

1. FEM analysis results accurately predict the fatigue crack initiation location, for which stresses and fatigue life were determined.

2. ALT can be used to get rapid test results on the rod life distribution. The symmetric sine load spectrum can be reduced to pulsating one, according to the stress spectrum analysis of the critical node.

3. Fatigue bench test revealed that the fatigue crack initiated from the rod inner edge and propagated along the cross section of the first pinhole, resulting in the fracture of the pinhole wall. The predetermined local stress and the fatigue life of the push rod calculated via FEM analysis agreed fairly well with the fatigue bench test results.

1. S. K. Koh, "Fatigue analysis of an automotive steering link," *Eng. Fail. Anal.*, **16**, No. 3, 914–922 (2009).

2. R. I. Stephens, A. Fatemi, R. R. Stephens, and H. O. Fuchs, *Metal Fatigue in Engineering*, Wiley, New York (2002).

3. J.-W. Han, J.-D. Kim, and S.-Y. Song, "Fatigue strength evaluation of a bogie frame for urban maglev train with fatigue test on full-scale test rig," *Eng. Fail. Anal.*, **31**, 412–420 (2013).

4. J.-S. Kim, "Fatigue assessment of tilting bogie frame for Korean tilting train: Analysis and static tests," *Eng. Fail. Anal.*, **13**, No. 8, 1326–1337 (2006).

5. M. M. Topaç, S. Ercan, and N. S. Kuralay, "Fatigue life prediction of a heavy vehicle steel wheel under radial loads by using finite element analysis," *Eng. Fail. Anal.*, **20**, 67–79 (2012).

6. E. A. Davis and F. M. Connelly, "Stress distribution and plastic deformation in rotation cylinders of strain-hardening material," *J. Appl. Mech.*, **26**, 25–30 (1959).

7. S. Özsoy, M. Çelik, and F. Suat Kadıoğlu, "An accelerated life test approach for aerospace structural components," *Eng. Fail. Anal.*, **15**, No. 7, 946–957 (2008).